Smart Structures and Systems, *Vol. 24, No. 2 (2019) 183-191*
DOI: https://doi.org/10.12989/sss.2019.24.2.183

Design and fabrication of a new piezoelectric paper feeder actuator without mechanical parts

Shahryar Ghorbanirezaei[*1], Yousef Hojjat[1a] and Mojtaba Ghodsi[2b]

[1]*Department of Mechanical Engineering, Tarbiat Modares University, Jalal Ale Ahmad, No. 7, Iran*
[2]*Department of Mechanical and Industrial Engineering, Sultan Qaboos University, Al Khoudh, No. 123, Oman*

(Received June 19, 2018, Revised April 18, 2019, Accepted April 21, 2019)

Abstract. A piezoelectric paper feeder actuator using Micro Virtual Roller (MVR) is proposed, designed, fabricated and tested. This actuator can drive a sheet of paper forward or backward without any mechanical parts, such as the costly and heavy rollers used in traditional paper feeders. In this paper feeder actuator, two vibrating stators which produce traveling waves are used to drive the paper. The vibrations of the stators are similar to those of piezoelectric motors and follow a similar procedure to move the paper. A feasibility study simulated the actuator in COMSOL Multiphysics Software. Traveling wave and elliptical trajectories were obtained and the dimensions of the stator were optimized using FEM so that the paper could move at top speed. Next, the eigenfrequencies of the actuator was determined. Experimental testing was done in order to validate the FEM results that revealed the relationships between speed and parameters such as frequency and voltage. Advantages of this new mechanism are the sharp decrease in power consumption and low maintenance.

Keywords: piezoelectric paper feeder actuator; piezoelectric motors; Micro Virtual Roller (MVR); elliptical trajectories; traveling wave

1. Introduction

Piezoelectric materials are used in, but are not limited to, new piezoelectric-based sensors, actuators and motors. Venkata and Raja (2014) examined the bending behavior of smart sandwich beams for health monitoring by considering debonding, boundary characteristics, actuation types and damage in their design procedures. Marinkovic (2012) analyzed the consequences of FEM mesh distortion on the numerical results when piezoelectric patches that are polarized in the thickness direction are used as actuators and sensors in thin-walled laminates.

Arefi and Rahimi (2012) reported that functionally graded piezoelectric annular plates with two smart layers (actuator and sensor) under a normal load and symmetric conditions should be considered to be nonlinear instead of linear. Rama (2017) proposed and validated a linear 3-node piezoelectric shell element for analysis of the linear and geometrically nonlinear dynamics of smart structures composed of composite laminates consisting of passive and multi-functional materials. An efficient 3-node shell element was developed by Marinković and Rama (2017) to numerically model piezoelectric laminated composite structures. The co-rotational FE formulation was exploited to explain the geometrically nonlinear effects. Zeng *et al.* (2014) proposed a 2D electro-static model to forecast the distribution of the stress of a piezoelectric actuator by studying the elastic body. Other researchers also have studied piezoelectric properties. When controlling vibrations of cantilevered plates instrumented with piezoelectric patches, the importance of considering changes in the piezoelectric coefficient and dielectric constants under different electrical fields was proved by Sharma *et al.* (2015).

Lin and Xu (2018) proposed a novel cascade sandwiched piezoelectric ultrasonic transducer which could be utilized for high power ultrasonic uses such as for ultrasonic machining and welding. Sung and Tien (2015) proposed a mathematic model to describe the sound field and vibration behavior of ultrasonic transducers. Zenz *et al*. (2013) compared passive and active methods of controlling and reducing noise in piezoelectric devices, especially transducers. Their optimum model reduced noise up to 20 dB in fabricated modal and nilpotent transducers. Zhou *et al*. (2016) proposed analytical formulae and FEM properties for the anisotropic piezoelectric transducer utilized for Lamb wave applications, such as for passive damage.

An important application for piezoelectric materials is in piezoelectric motors, also called ultrasonic motors, which are the focus of the current study. In rotary ultrasonic motors (RUSMs), the inverse piezoelectric effect is used to produce stator vibrations. Its vibrations make a traveling wave and elliptical motions on the surface of the stator. The rotor is mounted on a stator and preloading between the stator and rotor provide good friction at the contact surface; thus, the rotor begins to rotate against the direction of the traveling wave. This is possible in the stator when pieces of piezoelectric material from the stator are excited.

∗Corresponding author, MSc.
E-mail: Shahryar.ghorbani@modares.ac.ir
[a] Professor
[b] Assistant Professor

http://www.techno-press.com/journals/sss&subpage=7 ISSN: 1738-1584 (Print), 1738-1991 (Online)

Modeling of a RUSM was done by Hagood and McFarland (1995) and linear piezoelectric motors (LUSMs) have been developed by Sashida (1998) in which the slider (instead of the rotor) would drive linearly forward or backward. The pressure between the stator and slider in the LUSM (or stator and rotor in a RUSM) plays a central role in the movement of slider (or rotor). This role is directly related to friction force. Wallaschek (1998) revealed the relationship between contact and friction force. An S-Q ultrasonic motor was developed by Yoshita and Okamoto (2002) with a top speed of 10 mm/sec. Zhao (2011) developed a motor using in-plane modes with a maximum speed of 50 mm/sec at an operational voltage of 250 V. Hojjat and Karafi (2010) developed a roller interface ultrasonic motor (RIUSM) using rollers between the teeth of a stator. All of their rollers had two contact areas, which increased power.

A small bionic footstep piezoelectric motor was proposed by Li (2001) which attained a maximum speed of 90 mm/sec. A modified ultrasonic linear motor was developed by Zhai *et al.* (2000) that attained a top speed of 35 mm/sec. A frog-shaped linear piezoelectric motor working in only first-order longitudinal vibration mode was fabricated by Zhang *et al.* (2017) which was able to move a slider forward at a speed of 287 mm/sec. Tavallaei *et al.* (2016) presented a model for design of two robust inverse dynamic controllers to address the inaccurate motion of an ultrasonic motor under temperature disturbance. Pan *et al.* (2016) presented an ultrasonic motor with the highest speed and low friction which was able to rotate at 9120 r/min.

Applications of piezoelectric motors are not limited to these cases. Paik *et al.* (2009) developed a new type of multilayer piezoelectric linear ultrasonic motor for a camera module. The maximum speed was 35 mm/sec. Some applications for these motors include auto-focusing in cameras using a contact mechanism as developed by Maeno *et al.* (1990), as well as their use in watches, as done by Iino *et al.* (2000). Sadeghbeigi and Razfar (2013) developed an optimum load-speed diagram (and optimum design) for a LUSM which works in both the axial and flexural modes and used the softer cell-based smoothed finite element method (CS-FEM) to improve the performance of the piezoelectric motor.

In this study, a new application for piezoelectric motors is presented. A novel piezoelectric paper feeder based on the elliptical motion of the stators is proposed in which the shear vibrations of piezoelectric material are employed. These elliptical motions work similarly to rollers in printers and copy devices. The elliptical motions have been termed "Micro Virtual Roller (MVR)". The aim is the elimination of mechanical parts like rollers and guides used as traditional methods of moving paper forward in printers and copy devices. A sheet of paper has been substituted for the LUSM slider. Instead of rollers, stators are used that can drive a sheet of paper forward or backward between them. A feasibility study was done in COMSOL Multiphysics Software using FEM and the traveling wave and MVRs were determined for the stator. The dimensions of the stator have been optimized so that the MVRs would create the maximum tangential amplitude to move the paper at top speed. The eigenfrequencies and resonant frequency of the optimized actuator also has been determined. A piezoelectric paper feeder was fabricated and experimental tests were carried out to validate the FEM results of such a feeder. The relationships between speed and different parameters were determined through experimental testing.

2. Piezoelectric paper feeder actuator based on MVRs

A piezoelectric paper feeder actuator using MVRs is proposed that is able to drive a sheet of paper forward or backward. A simple schematic diagram is shown in Fig. 1. In this figure, two vibrating stators can move a sheet of paper backward or forward using MVRs created on the surfaces of the stators. Eight of these are shown in Fig. 1. Fig. 2 shows another schematic diagram of a stator with teeth. Fig. 3 shows that, in practice, each piezoelectric piece is separate from its adjacent piece, although Figs. 1 and 2 show one integrated piezoelectric piece. Fig. 3 shows an instance of a stator with four separate piezoelectric pieces. The stators are secured onto fixtures and thus, the method of fixing them should be addressed.

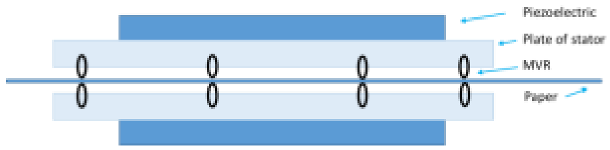

Fig. 1 Schematic diagram of potential stator and a sheet of paper in a piezoelectric paper feeder actuator using MVRs

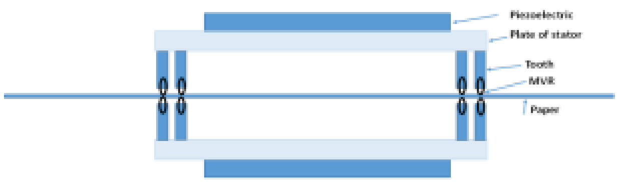

Fig. 2 Second schematic diagram of a stator having teeth with a sheet of paper in a piezoelectric paper feeder actuator using MVRs

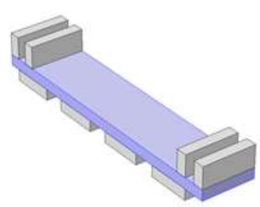

Fig. 3 Separate piezoelectric pieces in schematic diagram of the actuator

There were two methods available for the design of the feeder. First, the upper stator is secured on an upper fixture and the paper runs under the stator (in place of rollers on traditional printers). It is also possible to use a lower stator under the paper. The two stators work together to drive the sheet of paper. In this first method, guides are also required to direct the paper. The drawing of the stator and guides in this method is shown in Fig. 4. The upper stator only is shown in the figure. The paper moves between guides located on either side of the sheet. In the second method, two upper stators are secured on the upper fixture and two lower stators are secured on the lower fixture. Fig. 5 shows a drawing of this method in which only the upper stators are shown. The guides have been removed and two edge sensors are used to direct the paper. When the paper deviates from the straight direction to the left, the left sensor will sense this deviation and a controlling circuit will turn off the lower and upper stator on the right side. The left side stators (upper and lower) work alone to correct the direction. If the paper then deviates to the right side, all left stators will be turned off and only the right stators will remain on to reorient the paper. After several such adjustments, the paper will be able to move the entire distance as shown in Fig. 6. This system was inspired by the movement of military tanks.

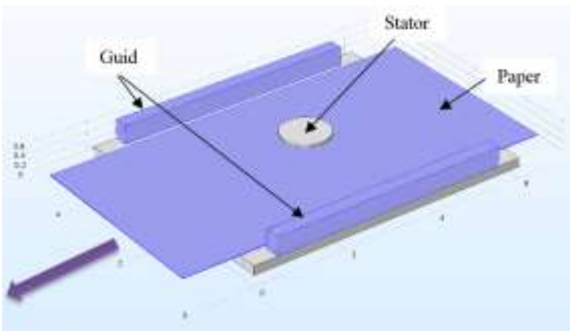

Fig. 4 First proposed method in which an upper stator is used. A lower stator can also be used under the paper

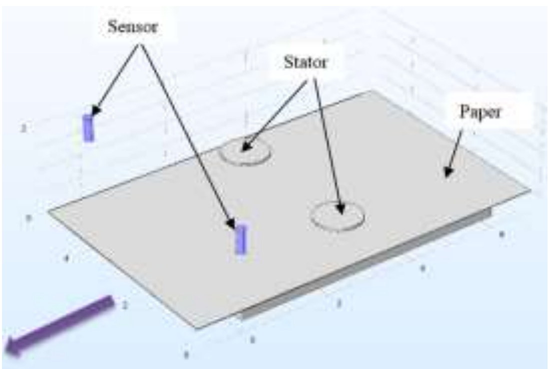

Fig. 5 Second proposed method in which two upper stators and two sensors are used. Lower stators are not shown

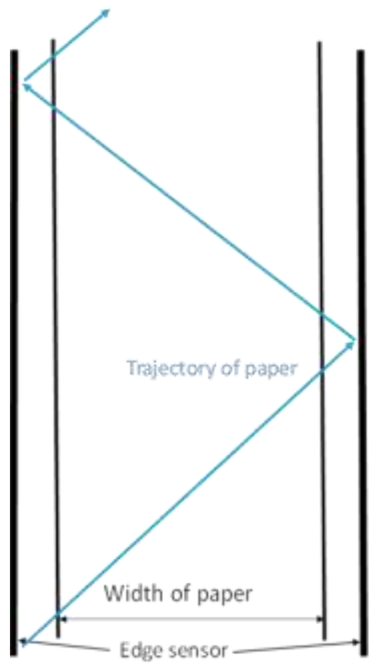

Fig. 6 Trajectory of paper in second method as inspired by military tank movement

3. Finite element analysis

To understand the feasibility of a piezoelectric paper feeder actuator based on MVRs, FEM analysis was done in Comsol Multiphysics Software. The ability to create a traveling wave and MVRs on the surface of stator with teeth was examined. FEM analysis for the models with and without teeth showed that the existence of teeth on the surface of a stator will increase the tangential amplitude which could increase the speed of paper and the normal amplitude, which can help preload the paper. The simulation also shows that the geometry of stator should be round –instead of possible rectangular in Fig. 3- to achieve greater MVR amplitude. The final drawing depicts a round feeder actuator with teeth. Fig. 7 shows different drawings of the stator, its parametric values and the MVRs of the traveling wave. The piezoelectric pieces are made of lead zirconate titanate 5-A (PZT 5-A) which its properties are shown in Table 1. The plate of the stator and its teeth are made of copper and a composite of polyurethane and steel fibers, respectively. FEM analysis followed two steps.

Table 1 PZT 5-A propertie

Poisson's Ratio	Density ($\times10^3$ Kg/m^3)	Youngs Modulus ($\times10^{10}$ N/m)		Piezoelectric Voltage Constants ($\times10^{-3}$ Vm/N)		Coupling Factors			Piezoelectric Charge Constants ($\times10^{-2}$ m/V)	
σ	ρ	YE 11	YE 33	g33	g31	Kp	K33	K31	d33	d31
0.35	7.6	7.4	5	27	-11	0.62	0.71	0.34	450	-175

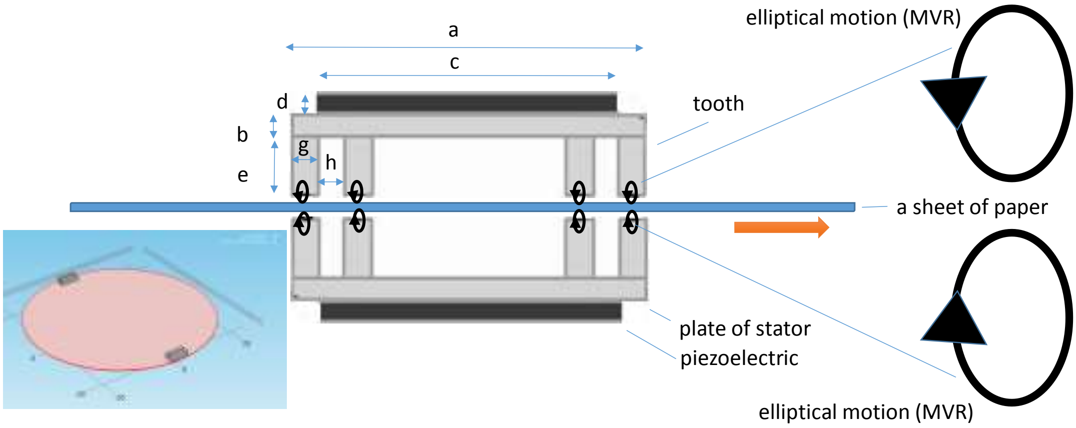

Fig. 7 Parametric dimensions of stators

3.1 Analysis for determining optimal dimensions

The optimum dimensions of the stator were determined by examining the behavior of each point on the surface of the stator as each piezoelectric piece is excited with sinuous voltage at a phase shift of 90° from the adjacent piece. The amplitude of the voltage is denoted as V0 and the simulation showed that the optimum size was independent of voltage amplitude. The simulation model and voltages of piezoelectric pieces are shown in Fig. 8. The free triangular mesh is used and the element size is fine. The minimum element size is 0.003 mm and the maximum element size is 0.8 mm. Maximum element growth rate is 1.2. The model is calibrated for general physics. The sparse matrix direct solver and nonlinear method were chosen "MUMPS" and "Automatic (Newton)", respectively. The MVRs were created by a traveling wave on the surface of the stator. Table 2 shows final optimized dimensions of the stator with considering the constant distance of 0.05 mm between electrodes. MVRs with and without teeth are shown in Fig. 9.

(a) FE model with triangular mesh

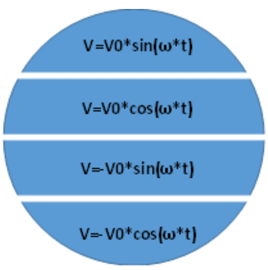

(b) Voltage of four piezoelectric pieces

Fig. 8 A section of FE model and applied voltages

Table 2 Optimized sizes of stators using parameters from Figs. 7 and 8

a	b	c	d	e	g	h
50 mm	0.2 mm	24 mm	0.2 mm	1.4 mm	0.8 mm	1.1 mm

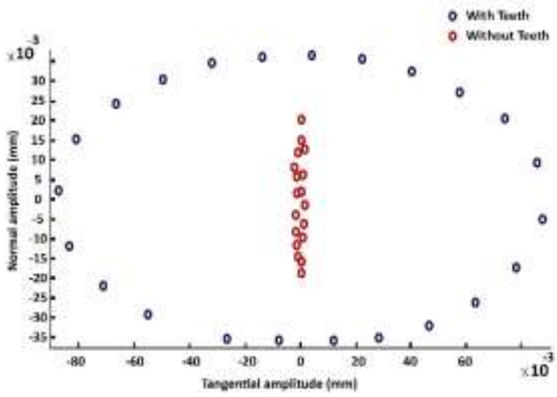

Fig. 9 MVR with teeth. Red curve denotes MVR (elliptical trajectory) on surface of a stator without teeth. Blue curve denotes MVR on one tooth of an optimized stator; all other teeth produce similar motions. Other stator sizes created curves of lower amplitude

3.2 Modal analysis

The optimized stator was modeled in Comsol Multiphysics to determine its ten eigenfrequencies. This analysis was carried out in Solid Mechanical Physical Environment, Modal Analysis Study. The second eigenfrequency was 2248 Hz.

4. Experimental testing

An actuator was fabricated to validate the simulation results. Experimental testing showed that the best mounting method to support the stator was a central support. Experimental work is presented in two sections.

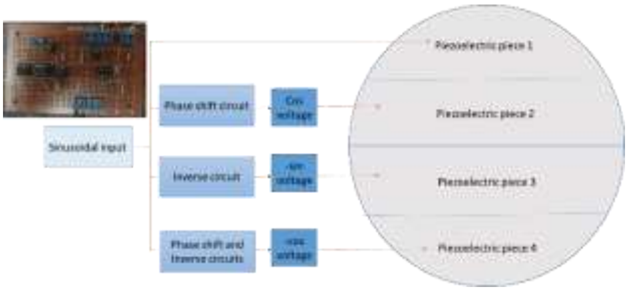

Fig. 10 Circuits that provide each piezoelectric piece with suitable voltage to form traveling waves and MVRs on surface of the teeth of the stator

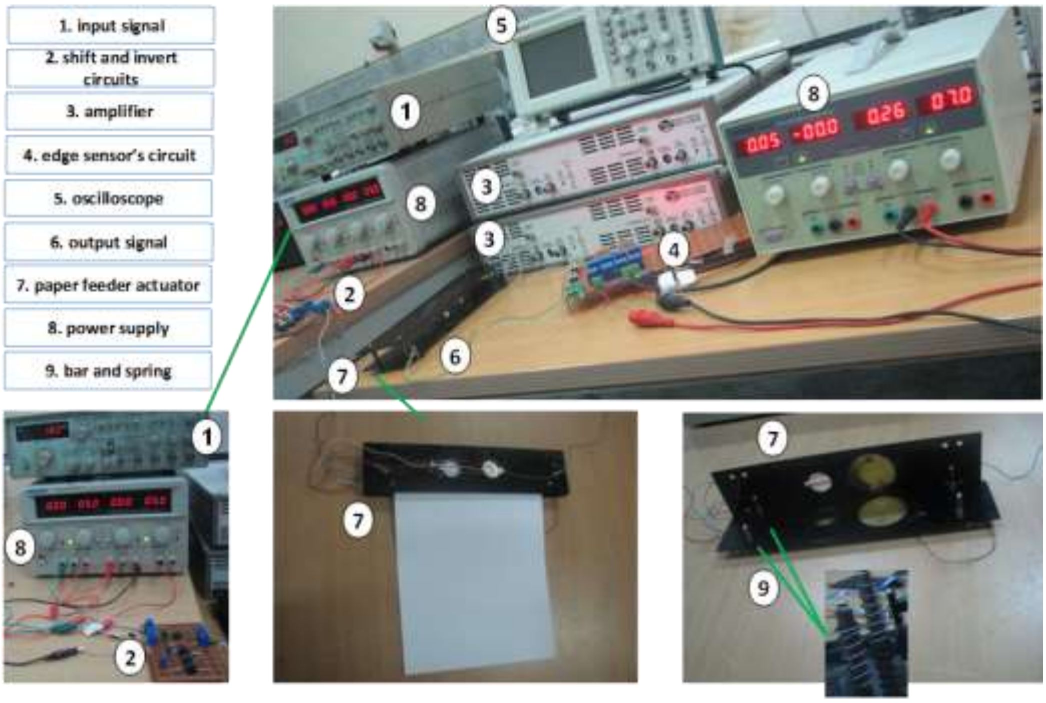

Fig. 11 Experimental set-up of first and second methods. The first method has no circuit to receive sensor signals. The second method uses two pairs of stators instead of one pair

4.1 Digital concept and controlling circuits of the actuator

Each piezoelectric piece was separate from the adjacent piece. Each piece, as specified in the simulation, was driven with sinuous voltage with a phase shift of 90° from the adjacent piece (Fig. 8). Sinusoidal input voltage drives the first piezoelectric piece. A phase shift circuit converts another sinusoidal voltage to a cosine voltage, which then drives the second piezoelectric piece. Two phase inverse circuits were applied to invert the sinusoidal and cosine voltages and they drove the third and fourth piezoelectric pieces, respectively. The schematic model of these circuits, the fabricated circuits and the whole process of creating appropriate voltages are shown in Fig. 10. These four circuits connect to four piezoelectric pieces attached to the stator. The controlling voltages were used to create a traveling wave in the stators and every point of the teeth experienced MVRs.

The experimental set-ups of the first and second methods are fairly similar and are shown in Fig. 11. In the first method, the rollers have been eliminated and, in the second method, both the rollers and guides have been eliminated and there was no contact between the guides and the paper. Thus, the guides have been inserted as far as possible from the paper (four holes of 5 mm in diameter in the fixture near the edge of the fixture) and the guides have been inserted into those holes. Two pairs of stators were used and, in place of guides, two edge sensors were used. The right sensor detects paper movement to the right and the left sensor detects paper movement to the left. In two deviations –either right or left- control circuit will operate. As shown in Fig. 12, if the green alarm for the right sensor turns on, it means that the paper has deviated to the right, the control circuit will turn off the left pair of sensors and turn on the right pair of stators. If the red alarm for the left -sensor turns on, it means that the paper has deviated to the left; thus, the right pair of stators will turn off and only the

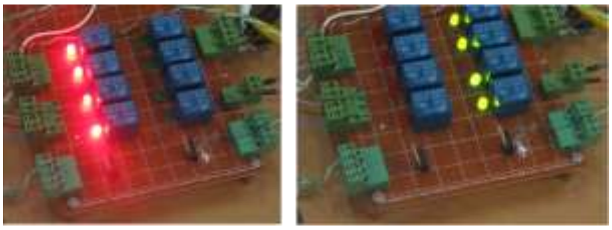

Fig. 12 Green alarm denotes edge sensor sensing a deviation toward the right. Red alarm denotes edge sensor sensing a deviation to the left. This circuit is number 4 in Fig. 11

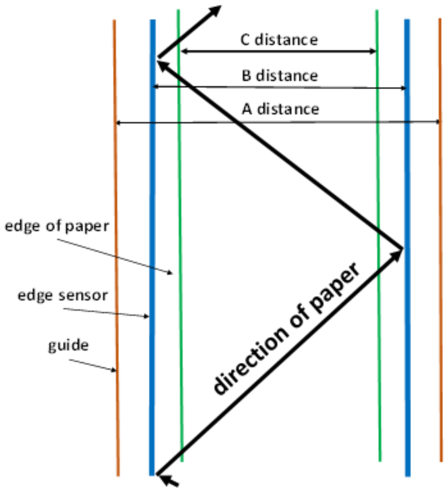

Fig. 13 Paper movement in second method. A denotes distance between guides, B denotes distance between two edge sensors and C denotes width of paper

left pair of stators will turn on. The paper will move as shown in Fig. 13 in which A is the distance between two guides, B is the distance between two edge sensors and C is the width of the sheet of paper. It can be seen in the figure that the distance between the sensor and the edge of the paper is a key factor. The relation between this distance and the speed of the paper was studied to determine the best distance and the results will be presented in section 5.

4.2 Fixture systems

Each stator was attached to a fixture that held it firmly in place as shown in Fig. 11. It was made of Fiberglass. The upper stator should be placed exactly above the lower stator; thus, a system for positioning them is required. The-one developed uses steel guide bars with surrounding steel springs (number 9 in Fig. 11). The guides in first method direct the movement of the paper and position the lower fixture exactly below the upper fixture. In the second method, the guides only perform the second role; only positioning fixtures and stators. The goal is to eliminate the guides directing the paper and use edge sensors instead. These fixtures and guide bar holes, which were 5 mm in diameter, are shown in Fig. 14. The four holes shown are 217 mm apart and are used for the first method. Four holes that are more than 217 mm apart were used for the second method. Fig. 14 shows the two holes of 25 mm in diameter were made in every fixture. In the first method, one hole in each fixture was used to place one stator. In the second method, two holes were used to place the two stators.

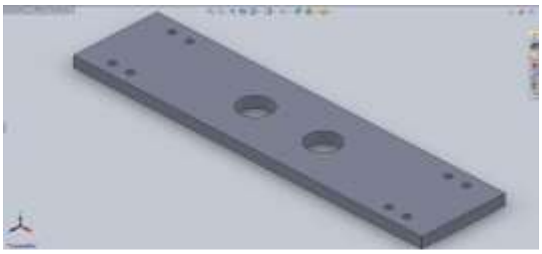

(a) 3-D view

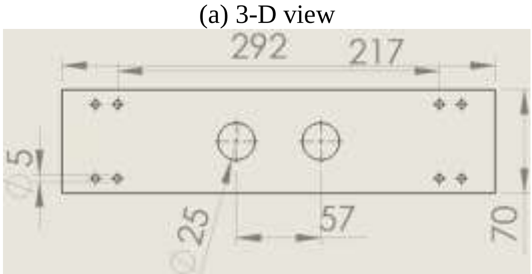

(b) sizes of fixtures

Fig. 14 Fixture used to secure stators

The mechanism is provided with a preload by applying weights to the fixture. The role of the preload was to provide normal force to create an appropriate friction force between the teeth of the stators and the paper.

5. Experimental results

It was observed that the energy consumption in the second proposed method was much lower than in the first method. A reason for this reduction is the decrease in friction and contact in the second method; thus, the remaining tests were carried out using the second method. These experimental tests determined the operating frequency, distance between B and C, voltage and preloading required to achieve the top speed of the sheet of paper. All tests were done with a sheet of paper with a mass of 5 g, except the test to determine the relationship between the mass of the paper and speed. The speed was determined from the time at which the last point of the sheet left the actuator.

5.1 Resonant frequency

The speed of paper was tested for a wide range of frequencies and it was found that the paper moves in a range of 1990 to 2490 Hz. This was tested by 10 Hz steps. The speed of the sheet was measured at each step, and ten points of them are shown in Fig. 15. The relationship between the frequency and speed of the sheet, which is shown in this figure, indicates the maximum speed happens at frequency of 2230 Hz. The parallel but lower curves were obtained at less than 125 V. This shows good agreement with the simulation results which indicates second eigenfrequency of 2248 Hz.

5.2 Relationship between speed and distance between B and C

Experimental tests showed that the distance between B and C (B-C in Fig. 13) had major effect on the speed of the paper; thus, the distance at which the paper moved at maximum speed was determined. In short distances, the sensors and controlling circuit were very sensitive and with a small deviation of paper, they would work and thus, they repeatedly turn on and off.

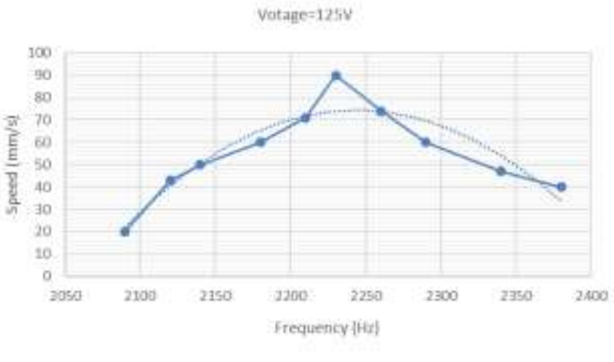

Fig. 15 Relationship between speed and frequency

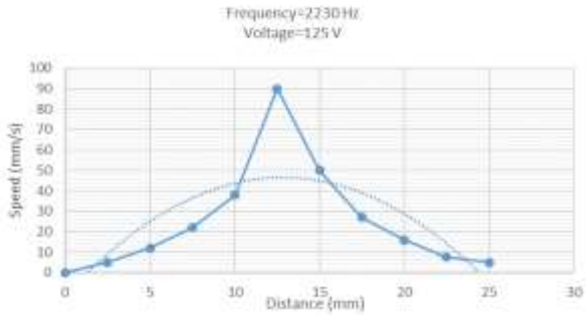

Fig. 16 Relationship between speed and distance between B and C (B-C)

In such short distances, no move of paper is made. On the other hand, in long distances, the paper would have, too much deviation and thus, the straight speed of paper would decrease.

Fig. 16 shows that the optimal distance between B and C was 12.5 mm. This distance is valid at all frequencies, voltages, preloadings, and weights of paper. This indicates that 12.5 mm is the optimal difference between B and C.

5.3 Relationship between speed and voltage

The relationship between speed and voltage was examined at a resonant frequency of 2230 Hz and B-C=12.5 mm. It was found that below 100 V, the speed of the sheet was very slow. Fig. 17 shows that the speed increased as the voltage increased. Moreover, the tests showed that when the voltage increased to above 125 V, the fatigue life of the stator fell sharply. The voltage at which the top speed of 90 mm/sec was achieved was 125 V. Note that the curves of all frequencies above and below the resonant frequency fell below this curve. This indicates that a resonant frequency of 2230 Hz caused the actuator to achieve the top speed.

5.4 Relationship between speed and preloading

The stators were secured to the upper and lower fixtures and the upper fixtures were weighted so that they would press the stators onto the paper.

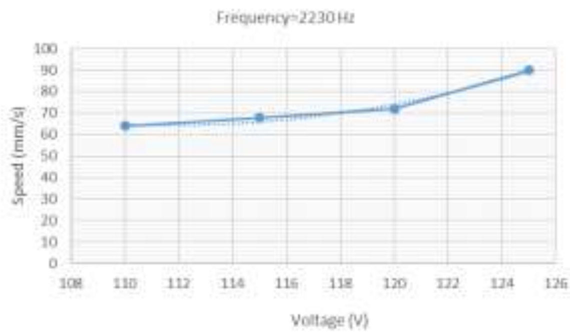

Fig. 17 Relationship between speed and voltage

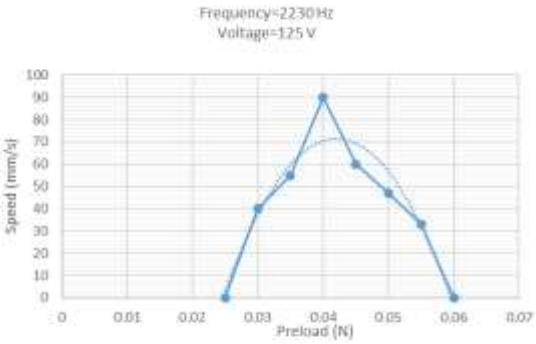

Fig. 18 Relationship between speed and preloading

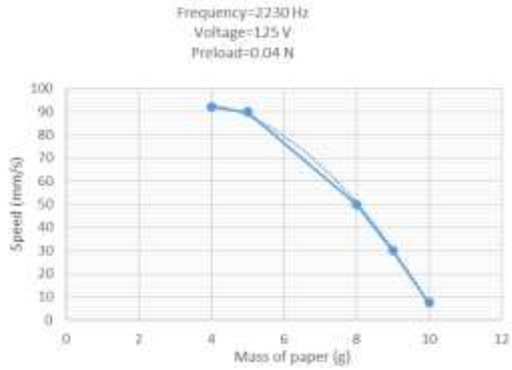

Fig. 19 Relationship between speed and mass of paper

The speed of the sheet of paper at various preloads was determined at a resonant frequency of 2230 Hz at 125 V. For a load of below 0.025 N the sheet moved very slowly. When the load reached 0.04 N, the sheet moved at a top speed of 90 mm/sec. This was determined to be the optimum force required to move the paper at top speed. For loads of more than 0.04 N, the speed decreased as the load increased. Fig. 18 shows the relationship between speed and preloading. All other curves at different frequencies and voltages fell below this curve and were parallel to it.

5.5 Relationship between speed and mass of paper

In addition to the frequency, voltage and preloading, the speed also depends on the mass of paper. The mass of paper in all previous tests was 5 g. In this experiment, papers with different masses of 4, 5, 8, 9 and 10 g were tested. The results for the range of masses are shown in Fig. 19. This figure shows the relationship between the speed and the mass of the sheet of paper. The experimental results indicated that the maximum speed of the sheet fell sharply at the higher masses. It can be suggested that the speed of the paper is maximized at a mass of 4 to 5 g.

6. Conclusions

The current study aimed to eliminate the mechanical components used to move a sheet of paper in printers and other copy devices by replacing the rollers with a piezoelectric paper feeder actuator based on Micro Virtual Roller (MVR). In the proposed system, two vibrating stators serve the same function as two rollers in a traditional device to move a sheet of paper forward or backward. Stators are similar to piezoelectric motor stators which produce a traveling wave and MVRs when four sinuous voltages (with a phase shift of 90°) are driven on each piezoelectric piece. The sheet of paper in this feeder actuator was substituted for the slider in the piezoelectric motors.

COMSOL Multiphysics Software was employed for a feasibility study to simulate the traveling wave and MVRs to drive the sheet of paper between two stators. The proposed mechanism was designed and optimized using FEM and the second eigenfrequency was found to be 2248 Hz.

An actuator was fabricated based on the optimized dimensions from FEM analysis to validate the simulation results. The actuator was experimentally tested and curves were produced for the speed of the sheet of paper versus the resonant frequency, distance between B and C, voltage, preloading and mass of paper. The resonant frequency of 2230 Hz showed good agreement with simulation results of 2248 Hz. Experimental results showed that the speed of a sheet of paper increased proportionally to an increase in voltage. The results in the simulation and the limitation of the thin piezoelectric piece in the experimental testing prevented the maximum value of voltage from being above 125 V; thus, this value was chosen as the final voltage. The experimental curves indicated that preloading of 0.04 N provided the maximum speed. It was also found that as the mass of the sheet of paper increased, its speed decreased. A maximum speed of approximately 90 mm/sec was achieved for paper with mass of 4 or 5 g. This actuator has been shown to be a light, very small and cost-effective viable alternative to traditional paper feeding systems.

References

Arefi, M. and Rahimi, G.H. (2012), "Studying the nonlinear behavior of the functionally graded annular plates with piezoelectric layers as a sensor and actuator under normal pressure", *Smart Struct. Syst.*, **9**(2), 127-143. https://doi.org/10.12989/sss.2012.9.2.127

Hagood, N.W. and McFarland, A.J. (1995), "Modeling of a piezoelectric rotary ultrasonic motor", *IEEE T. Ultrason. Ferr.*, **42**(2), 210-224. https://doi.org/10.1109/58.365235.

Hojjat, Y. and Karafi, M.R. (2010), "Introduction of roller interface ultrasonic motor (RIUSM)", *Sensor Actuat. A: Phys.*, **163**(1), 304-310. https://doi.org/10.1016/j.sna.2010.07.002

Iino, A., Suzuki, K., Kasuga, M., Suzuki, M. and Yamanaka, T. (2000), "Development of a self-oscillating ultrasonic micro-motor and its application to a watch", *Ultrasonics*, **38**(1-8), 54-59. https://doi.org/10.1016/S0041-624X(99)00192-4.

Li, C. (2001), "Small-sized bionic ultrasonic linear motor", *Small Spec. Machines*, **11**(6), 10-11.

Lin, S. and Xu, J. (2018), "Analysis on the cascade high power piezoelectric ultrasonic transducers", *Smart Struct. Syst.*, **21**(2), 151-161.

Maeno, T., Tsukimoto, T. and Miyake, A. (1990), "The contact mechanism of an ultrasonic motor", *Proceedings of the IEEE 7th International Symposium on Applications of Ferroelectrics*, Champaign, Illinois, United States, June. https://doi.org/10.1109/ISAF.1990.200308

Marinkovic, D. and Marinkovic, Z. (2012), "On FEM modeling of piezoelectric actuators and sensors for thin-walled structures", *Smart Struct. Syst.*, **9**(5), 411-426. https://doi.org/10.12989/sss.2012.9.5.411

Marinkovic, D. and Rama, G. (2017), "Co-rotational shell element for numerical analysis of laminated piezoelectric composite structures", *Compos. Part B: Eng.*, **125**, 144-156. https://doi.org/10.1016/j.compositesb.2017.05.061

Paik, D.S., Yoo, K.H., Kang, C.Y., Cho, B.H., Nam, S. and Yoon, S.J. (2009), "Multilayer piezoelectric linear ultrasonic motor for camera module", *J Electroceram*, **22**(1-3), 346-351.

Pan, Q., Huang, F., Chen, J., He, L.G., Li, W. and Feng, Z. (2016), "High-speed low- friction piezoelectric motors based on centrifugal force", *IEEE T. Ind. Electron*., **64**(3), 2158- 2167. https://doi.org/10.1109/TIE.2016.2623578.

Rama, G. (2017), "A 3-node piezoelectric shell element for linear and geometrically nonlinear dynamic analysis of smart structures", *Facta Universitatis-Series Mechanical Engineering*, **15**(1), 31-44.

Rama, G., Marinković, D. and Zehn, M. (2017), "Efficient three-node finite shell element for linear and geometrically nonlinear analyses of piezoelectric laminated structures", *J. Intel. Mat. Syst. Str.*, **29**(3), 345-357. https://doi.org/10.1177%2F1045389X17705538

Sadeghbeigi Olyaie, M. and Razfar, M.R. (2013), "Numerical characterizations of a piezoelectric micromotor using topology optimization design", *Smart Struct. Syst.*, **11**(3), 241-259. https://doi.org/10.12989/sss.2013.11.3.241.

Sashida, T. (1998), *An Introduction to Ultrasonic Motors*, Oxford university press, Oxford, United Kingdom.

Sharma, S., Vig, R. and Kumar, N. (2015), "Active vibration control: considering effect of electric field on coefficients of PZT patches*", Smart Struct. Syst.*, **16**(6), 1091-1105. https://doi.org/10.12989/sss.2015.16.6.1091

Sung, C. and Tien, S. (2015), "The study on piezoelectric transducers: theoretical analysis and experimental verification", *Smart Struct. Syst.*, **15**(4), 1063-1083. https://doi.org/10.12989/sss.2015.15.4.1063

Tavallaei, M.A., Atashzar, S.F. and Drangova, M. (2016), "Robust motion control of ultrasonic motors under temperature disturbance", *IEEE T. Ind. Electron*. **63**(4), 2360 – 2368. https://doi.org/10.1109/TIE.2015.2499723.

Venkata Rao, K., Raja, S. and Munikenche, T. (2014), "Finite element modeling and bending analysis of piezoelectric sandwich beam with debonded actuators", *Smart Struct. Syst.*, **13**(1), 55-80. http://dx.doi.org/10.12989/sss.2014.13.1.055

Wallaschek, J. (1998), "Contact mechanics of piezoelectric ultrasonic motors", *Smart Mater. Struct.*, **7**(3), 369–381. https://doi.org/10.1088/0964-1726/7/3/011

Yoshita, R. and Okamoto, Y. (2002), "Micro piezoelectric actuator'', *J. Japan society for precision Eng*., **68**(5), 645-648.

Zeng, X., Yue, Z., Zhao, B. and Wen, S.F. (2014), "Analysis of a three-dimensional FEM model of a thin piezoelectric actuator embedded in an infinite host structure", *Adv. Mater. Res*., **3**(1), 237-257. https://doi.org/10.12989/amr.2014.3.1.237

Zenz, G., Berger, W., Gerstmayr, J., Nader M. and Krommer M. (2013) "Design of piezoelectric transducer arrays for passive and active modal control of thin plates", *Smart Struct. Syst.*, **12**(5), 547-577. https://doi.org/10.12989/sss.2013.12.5.547.

Zhai, B., Lim, S.P., Lee, K.H., Dong, S. and Lu, P. (2000), "A modified ultrasonic linear motor", *Sensor Actuat. A: Phys*., **86**(3), 154-158. https://doi.org/10.1016/S0924-4247(00)00439-8

Zhang, Q., Chen, W., Liu, Y., Liu, J. and Jiang, Q. (2017), "A frog shaped linear piezoelectric actuator using first order longitudinal vibration mode", *IEEE T. Ind. Electron*., **64**(3), 2188-2195. https://doi.org/10.1109/TIE.2016.2626242.

Zhao, C. (2011), *Ultrasonic Motors Technologies and Applications*, (2nd Ed.), Science press Beijing, Nanjing, Jiangsu, China.

Zhou, W., Li, H. and Yuan, F.G. (2016), "An anisotropic ultrasonic transducer for Lamb wave applications", *Smart Struct. Syst*., **17**(6), 1055-1065. https://doi.org/10.12989/sss.2016.17.6.1055.

HJ